High-Bandwidth High-Temperature (250 °C / 500 °F) Isolated DC and AC Current Measurement: Bidirectionally Saturated Current Transformer

B. Wrzecionko,
L. Steinmann,
J. W. Kolar

High-Bandwidth High-Temperature (250 °C/500 °F) Isolated DC and AC Current Measurement: Bidirectionally Saturated Current Transformer

Benjamin Wrzecionko, *Student Member, IEEE*, Lukas Steinmann, and Johann W. Kolar, *Fellow, IEEE*

Abstract—In an increasing number of application areas and industry sectors, such as the automotive, aerospace, military or oil and gas industry, a trend towards higher ambient temperature rating from 85 °C upwards for electrical machines and power electronic converters can be observed. To reduce the impact of high ambient temperatures on the power density, the interest in power electronic converters with SiC power semiconductors operated up to a junction temperature of 250 °C rises. The control of power electronic converters typically requires a precise, fast, and robust current measurement. However, analyzing current measurement concepts from the literature reveals that there is a lack of measurement systems, that are galvanically isolated and able to measure dc and higher frequency ac currents fast at high ambient temperatures of 250 °C. In this paper, a current measurement concept of a bidirectionally saturated current transformer is presented, that is able to measure dc and sinusoidal ac up to 1 kHz and 50 A at an ambient temperature of 250 °C with an relative error of 2.6% and less than 0.5% error after initial calibration. Furthermore, a prototype is designed, built, and used for the experimental verification of the concept.

Index Terms—Current measurement, current transformers.

I. INTRODUCTION

A TREND towards higher ambient temperature rating from 85 °C upwards for electrical machines and power electronic converters can be observed in an increasing number of application areas and industry sectors [2]–[4]. The automotive industry with the growing interest in hybrid electric vehicles (HEVs) [5], [6], the military or aerospace sector with future ambitious expeditions to, e.g., the Venus [7] or the oil and gas industry with the exploration of deeper reservoirs [8] can be given as examples.

Most state-of-the-art actual power electronic converters feature silicon (Si) power semiconductors and thus their junction temperature is subject to an upper temperature limit between 150

and 175 °C [9] due to the high intrinsic charge carrier concentration of Si for temperatures exceeding 175 °C [10]. In order to effectively remove the heat dissipated by the power semiconductor switches and maintain a reasonable size of the cooling system and thus reduce the impact of the high ambient temperature on the power density, a sufficiently large temperature difference between the semiconductor junction and the ambient has to be maintained. With silicon carbide (SiC), a new material that can be used for power semiconductor switches has become available. SiC switches are capable of significantly higher operating temperatures up to 400 °C [11]. Novel joining and bonding technologies such as low-temperature sintered silver die attachment and copper bonding instead of aluminum bonding are currently investigated and promise considerably improved reliability for thermal cycling with increased temperature swing [12]–[14].

Considering the example of an ambient-air-cooled power electronic dc–ac drive inverter for HEVs mounted under the engine hood [15], an ambient temperature of 120 °C can be assumed for the converter [5], [6]. To maximize the chip utilization and power density, a junction temperature around 250 °C for typical SiC power semiconductors at 120 °C ambient temperature has been shown to be close to the optimum junction temperature [16].

This means, also the signal electronics (including the current and voltage measurement), the passive components like dc-link capacitors as well as the components of the air-cooling system such as thermal interface materials, heat sinks, and fans need to withstand these harsh temperature conditions. For the signal electronics and passives, a converter setup dealing with the challenges induced by 120 °C ambient and 250 °C junction temperature is shown in [15] where the signal electronics and passives are thermally isolated from the power semiconductors and remain at the ambient temperature level of 120 °C. Thermally conductive interface materials are available up to 300 °C [17], heat sinks are typically made of aluminum or copper and thus can withstand these temperatures as well. An automotive fan for operation at an ambient temperature of 250 °C, that offers a comparable fluid dynamic performance for power electronics cooling as the best-in-class conventional fans, is presented in [18].

For a high-quality control of a power electronic converter, ideally the current is measured precisely and without time delay and/or with a high bandwidth. To avoid letting the load current flow through the thermally shielded part of the signal electronics part, the current can be directly measured at the power semiconductor packages, and hence the measurement needs to withstand temperatures of up to 250 °C [15]. Given the previous example
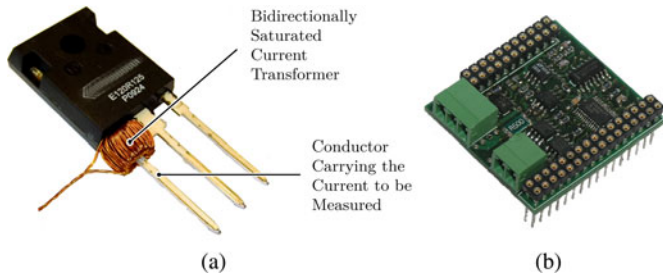
Fig. 1. (a) Photograph of the bidirectionally saturated current transformer [1] mounted on a discretely packaged SiC power semiconductor switch. (b) PCB with signal and small power electronics to magnetize the current transformer core from its secondary side. The PCB also contains connectors to the transformer itself and to the digital control platform of the overall converter system which employs the system for current measurement system.

TABLE I
SPECIFICATIONS OF THE CURRENT MEASUREMENT SYSTEM

Bidirectionally Saturated Current Transformer	
Current Measurement	-50 .. 50 A
Sin. Current Frequency Range	0 .. 1 kHz
Min. Measurement Frequency	50 kHz
Max. Op. Temperature	250 °C
Outer Diameter[1]	6.5 mm
Inner Diameter[1]	2.9 mm
Height[1]	5.5 mm

[1]Including secondary winding.

[15], for the signal electronics that comes possibly with a current measurement system, an ambient temperature capability of around 120 °C is sufficient if the control of the current measurement system can be separated from the actual measurement at the power semiconductors.

In recently published high-temperature converter systems such as [15] and [19], the current is measured using shunts that operate at 250 °C. The analog–digital converter (ADC) required for the digital control of the drive inverter can be placed in a thermally shielded signal electronics box operating at 120 °C. Shunts offer an easy and cheap measurement of both dc and ac currents (providing the option of monitoring the dc current drawn from the battery and the variable frequency ac output currents shaped by the inverter of an HEV using the same technology), but they are not galvanically isolated and thus their voltage signal must be isolated if the shunt potential can be different from that of the signal processing electronics. Additionally, shunts require for accurate operation over large temperature ranges a temperature compensation due to the temperature drift of the resistance. Furthermore, the voltage measured at their terminals can be easily distorted by EMI occurring in switch mode power electronic converters, especially when mounted close to the power semiconductor switches. If the measured current ranges from small to very large values, the resistor has to be chosen sufficiently high so the currents still lead to a measurable voltage while at the same time, large resistor while at the same time, large currents at the opposite end of the measurement range will lead to high power losses and thus even higher temperatures of the resistor.

Alternative current measurement concepts are shown in Fig. 2. For high ambient temperatures of 250 °C, Hall effect, magnetoresistive, and magnetoptical sensors cannot be used due to individual technological temperature limits. The concepts utilizing the magnetic flux in a coil or magnetic core caused by the current to be measured are generally more suitable for higher operating temperatures as the technology involved (windings and a ferro- or ferrimagnetic core) is available for these temperatures. However, some options of them suffer from other disadvantages: Rogowski coils and current transformers can only measure ac down to a lower cutoff frequency due to their operating principle based on the change of the magnetic flux. At low vehicle and thus rotational speeds of the electrical drive, the frequency of the output current in the range of less than 1 Hz is likely to be

below the lower cutoff frequency of the coil or the transformer. A Fluxgate sensor can generally be used for dc and ac measurements at high temperatures, but the upper cutoff frequency of the sensor is very limited by the control of the saturable inductor sensing the magnetic flux of the gapped core.

In this paper, the novel current measurement concept is based on a "bidirectionally saturated current transformer" is presented in Table I, which allows fast measurement also of sinusoidal currents at high ambient temperatures of 250 °C for power electronic converters with medium switching frequencies and nearly sinusoidal output currents (e.g., due to a high load inductance). The introduced concept shares some common features with the dc current transformer that is known for many years [20]–[22] but to make it suitable for measuring sinusoidal currents with frequencies of up to 1 kHz, it shows a modified magnetic design and is directly hardware controlled enabling significantly faster measurement than the usual dc measurement concepts and thus allowing to measure ac as well. The physical values measured to determine the current are also different to previously published concepts in order to eliminate any influence of the temperature. In Section II, the measurement principle, the differences to known concepts based on current transformers and the guidelines for selecting dimensioning a magnetic core for this measurement system are shown in detail. Subsequently, the realization and experimental verification of a measurement system are presented in Sections III and IV, respectively.

II. MEASUREMENT SYSTEM

A. Measurement Principle

The basic physical setup of the current measurement system is shown in Fig. 3(a). The current i_p which is to be measured is fed through a toroidal core made of ferro- or ferrimagnetic material with N_p primary turns. Provided the magnetic permeability μ of the core is by orders of magnitude higher than that of the surrounding medium (e.g., air), turnes. The unknown primary current i_p that is to be measured causes a magnetic field strength that is given by

$$H_p = \frac{i_p \cdot N_p}{l_m} \quad (1)$$

where l_m denotes the average length of the magnetic path in the core. The core radius and the saturation magnetic field strength H_{sat} of the core material are chosen so small that the minimum current $i_{p,min}$ that has to be measured leads to saturation of the core, i.e., to a value of $H_p > H_{sat}$.
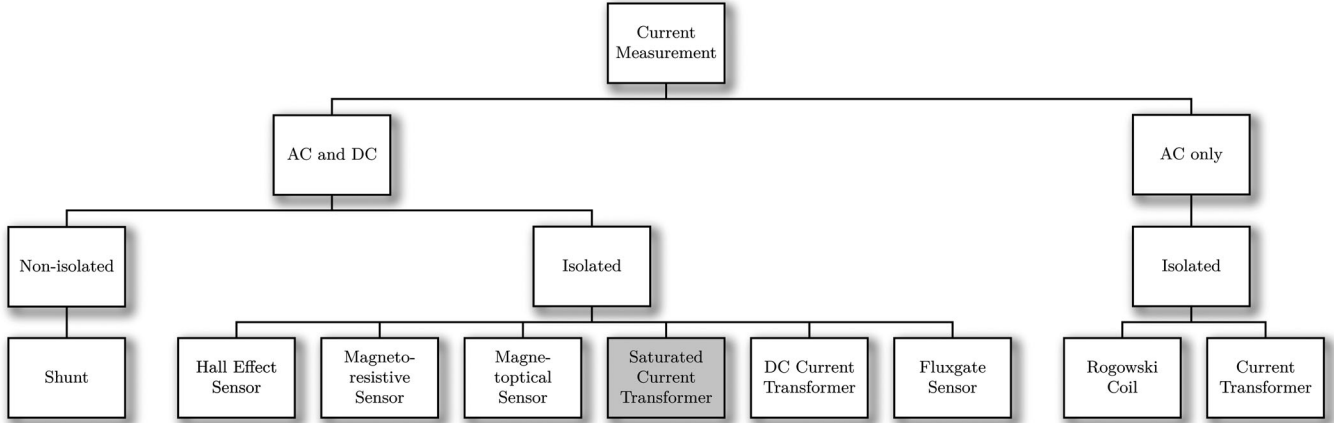
Fig. 2.   Overview of state-of-the art current measurement concepts: for ac and dc measurements in high-temperature applications, currently often shunts are used. Their measurement signal is not galvanically isolated, suffers from a temperature drift and can be easily distorted by EMI. For high ambient temperatures of 250 °C, Hall effect, magnetoresistive, and magnetoptical sensors cannot be used due to individual technological temperature limits. Rogowski coils and current transformers can only measure ac down to a lower cutoff frequency. The concepts utilizing the magnetic flux in a coil or magnetic core caused by the current to be measured are generally more suitable for higher operating temperatures. The new concept introduced in this paper is the "saturated current transformer,' that is able to measure dc and sinusoidal ac up to 1 kHz and 50 A at an ambient temperature of 250 °C.
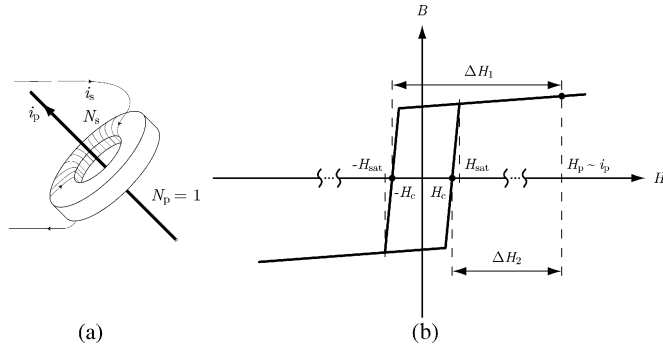

Fig. 3.   (a) Basic physical setup of the bidirectionally saturated current transformer: the (primary) current i_p to be measured is fed through a toroidal core that also carries a secondary winding. (b) Basic measurement principle: the primary current is determined using the mean value of the secondary currents that are needed to reach the coercive magnetic field strength $\pm H_c$ of the hysteresis loop.

As can be seen from Fig. 3(b), H_p can be calculated using the differences ΔH_1 and ΔH_2 in the magnetic field strength from H_p to the coercive magnetic field strength H_c:

$$H_p = \frac{\Delta H_1 + \Delta H_2}{2}. \tag{2}$$

The toroidal core also carries a secondary winding with N_s turns, driven by a full bridge (cf. Fig. 4) causing a secondary current i_s and a secondary magnetic field strength H_s in the core. The H-bridge is controlled such that the full hysteresis loop is traversed within one pulse period of the H-bridge by the magnetic field strength H_s which is superimposed on H_p. During traversing the hysteresis loop, the currents i_{s1} and i_{s2} corresponding to $-H_c$ and H_c, respectively, are measured using the shunt R_s and with

$$\Delta H_1 = \frac{i_{s1} \cdot N_s}{l_m}$$

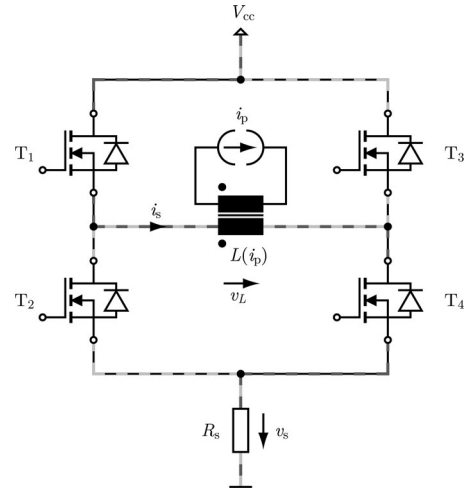$$\Delta H_2 = \frac{i_{s2} \cdot N_s}{l_m}, \tag{3}$$

Fig. 4.   Circuit diagram of the current measurement setup: the bidirectionally saturated current transformer is magnetized by a primary current i_p. The secondary winding on the toroidal core of the transformer is connected to an H-bridge and the secondary current i_s is measured by a shunt R_s. The gray current paths correspond to the current waveform shown in Fig. 5(b).

i_p can be finally calculated as

$$i_p = \frac{N_s}{N_p} \cdot \frac{i_{s1} + i_{s2}}{2}. \tag{4}$$

Hence, the magnetic setup should be viewed more an sensing element that senses the primary magnetic field H_p and thus the current i_p that is to be measured by the use of a secondary magnetic field H_s caused by an impressed secondary current i_s than as an actual current transformer.

In Fig. 5(a) and (b), the idealized traversing of the hysteresis loop is shown in detail. The single-phase inverter in Fig. 4 starts to apply the dc-link voltage V_{cc} to the secondary winding on the toroidal core at t_0. As the core is saturated by i_p and thus shows a relative permeability close to unity, the current i_s will rise fast.

Assuming that the direction of i_s leads to a flux that is opposing the flux caused by i_p, the increase will become less steep
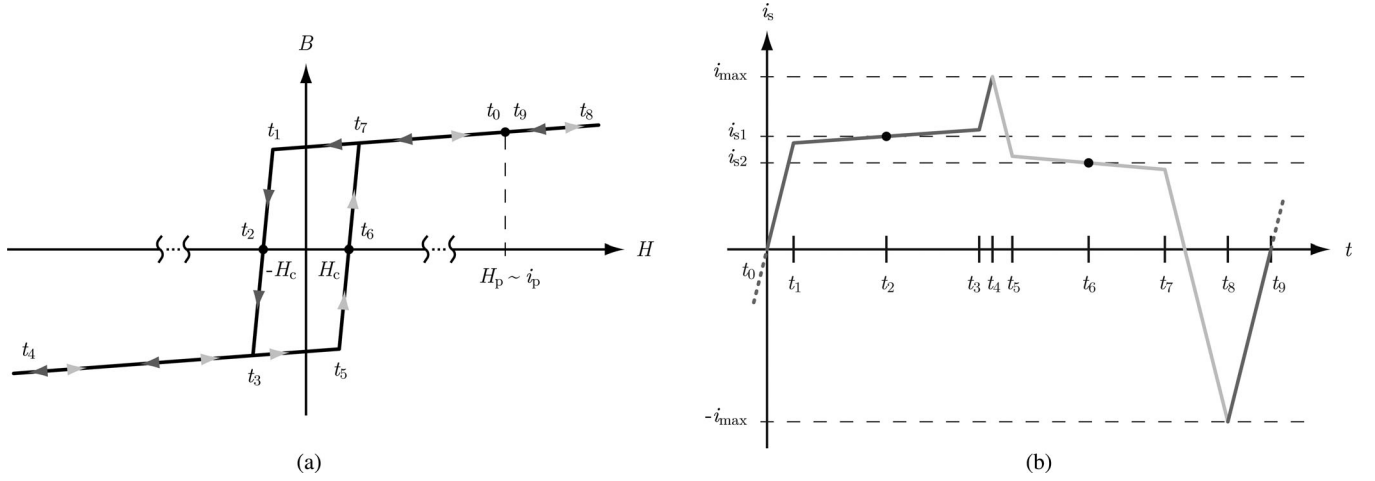
Fig. 5. Traversing the $B(H)$ hysteresis loop by proper modulation of the H-bridge shown in Fig. 4: the different operating points of the bidirectionally saturated current transformer within one pulse period of the H-bridge on the secondary side are shown on the hysteresis loop (cf. (a)) and secondary current waveform (cf. (b)).

once the sums of H_p and H_s add up to a value in between $-H_c$ and H_c which happens at time instant t_1. At t_2, $i_s(t = t_2) = i_{s1}$ needs to be measured. With a further increase in i_s, the core will reach saturation again at t_3, leading to a steep increase in i_s until a predefined current limit is reached and the voltage applied to the secondary winding is reversed at t_4 and the hysteresis loop is traversed in the opposite direction, measuring $i_s(t = t_6) = i_{s2}$ and having $i_s(t = t_9) = 0$ at t_9 where the switching period of the H-bridge starts again.

If the previous assumption that H_p and H_s are in opposite direction is wrong, the core will be saturated even further in the direction of H_p. Thus, the current limit of i_s (either i_{max} or $-i_{max}$) will be reached without desaturation of the core and thus also without any measurement of the secondary current and the H-bridge reverses the voltage so that the measurement cycle can start as described previously.

It can be seen in Fig. 5(b) that the time difference between t_7 and t_5 is smaller than between t_3 and t_1. The reason for this fact is illustrated in Fig. 6: when V_{cc} is applied to the secondary winding such that i_s rises [cf. Fig. 6(a)], the voltage drop caused by i_s across the parasitic resistances (drain–source on-resistance $R_{DS,on}$ of the MOSFETs in the H-bridge and the winding resistance R_{cu}) and across the shunt R_s reduces the voltage v_L applied to the secondary winding. Hence, it takes longer to build up the same inductor current, than it takes to make the inductor current decrease by applying V_{cc} in the opposite direction. This is true because i_s still flows in the same direction for both cases, but in the latter case, the voltage drop across the on-resistances of the other pair of switches and across R_s is added to V_{cc} and only the voltage drop across R_{cu} reduces v_L and thus the slope of i_s between t_1 and t_3.

This phenomenon can also be explained by the following consideration: the shunt is placed in the dc-link, and the load is purely inductive, if losses are neglected. Hence, the current through (or voltage across) the shunt should be free of a direct component. The second lowest waveform in Fig. 10 shows the
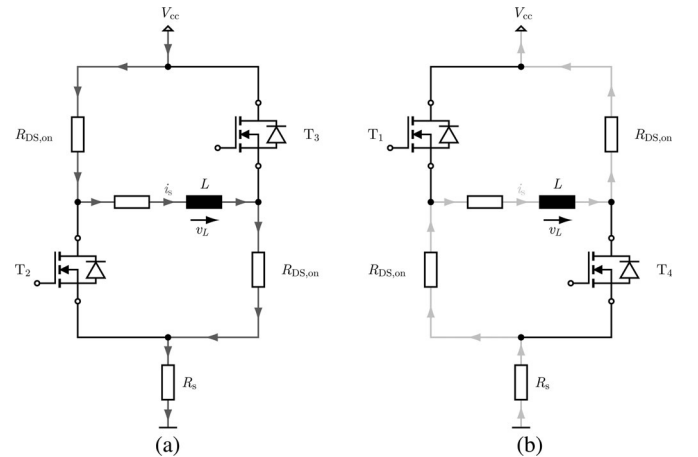

Fig. 6. Difference in inductor voltage depending on the switching state of the H-bridge: for a given direction of the primary current i_p, the direction of the secondary current i_s is independent of the switching state of the H-bridge, when the core is not saturated (i.e., during the time interval between t_1 and t_3 as well as between t_5 and t_7). Hence, in one switching state (a), the voltage v_L applied to the inductor is V_{cc} minus the ohmic voltage drops occurring due to $R_{DS,on}$, R_s, and R_{cu} and in the other switching state (b) v_L is the negative *sum* of V_{cc} and the voltages over $R_{DS,on}$, R_s, and R_{cu}. This means that the absolute voltage applied to the inductor is larger between t_7 and t_5 than between t_3 and t_1 and hence, the time interval between t_7 and t_5 is smaller than between t_3 and t_1 in Fig. 5.

shunt voltage for the secondary current as in Fig. 5(b). It can be seen that the direct component in the shunt voltage v_s is introduced only by the difference in time that is spent in the region where the core is not saturated, and is finally caused by the losses in the parasitic resistances.

B. Major Differences to Other Current Transformer Concepts

Measuring the secondary current at $\pm H_c$ is a significant difference to [21] where the secondary current is measured when the core starts to saturate. The latter is difficult to realize with typical ADCs as the current rises very fast once the core is saturated. How the crucial task of finding the right point in time
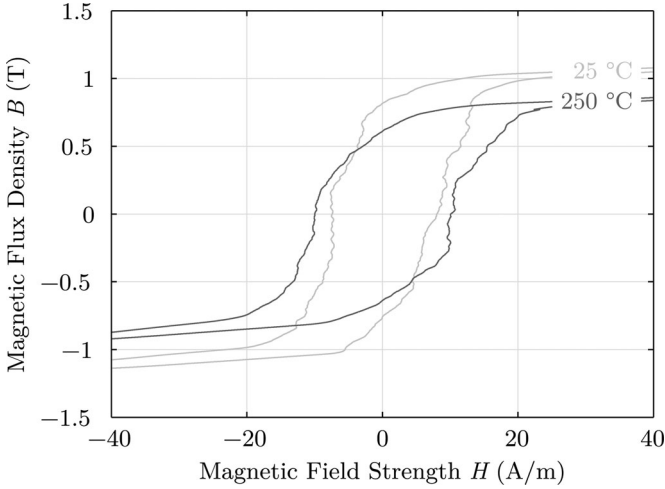
Fig. 7. Filtered hysteresis loop of "Vitroperm 500F" measured at 25 kHz and 25 and 250 °C using a "T60006-L2009-W914" core [22]. The material has been chosen because of a high μ_r of up to 150 000, a low coercive and saturation magnetic field strength as well as a high operating temperature capability of up to 300 °C and a comparably high temperature invariance of these magnetic parameters. Furthermore, the commercial cores available are tape wound and hence, the core dimensions can be easily adjusted to meet the needs of the experimental prototype of the bidirectionally saturated current transformer.

to sample the secondary current for the measurement principle presented in this paper can be tackled is shown in Section III-D.

In [21], it is proposed to calculate the primary current by measuring the time to saturation. The saturation flux density, which shows a significant temperature dependence for typical ferro- or ferrimagnetic core materials (cf., e.g., the hysteresis loop in Fig. 7), is needed in the resulting equation for i_p though. It can be seen from (4) that the measurement of i_p in the concept shown in this paper is invariant against temperature changes of the core as N_s and N_p are temperature independent.

For an ideally lossless core material, the area enclosed by the hysteresis loop would be zero leading to $H_c = 0$ and the difference in i_{s1} and i_{s2} would vanish. In reality, measuring i_{s1} and i_{s2} to find the mean value can lead to a more precise calculation of i_p using (4). Especially for high bandwidth and/or high excitation frequencies, this is particularly important due to $|H_c|$ increasing with frequency. Taking the width of the hysteresis loop into account when calculating the primary current is one important difference to [22].

C. Transformer Core

The choice of the transformer core material and design is crucial for the fast and precise operation of the current measurement system at ambient temperatures of 250 °C. It must be made sure that the important material parameters mentioned in this section are assessed in the whole temperature range from −40°C to temperatures above 250 °C as the core heats up to temperatures higher than the ambient temperature due to the losses occurring when traversing the hysteresis loop.

1) Relative Permeability μ_r: As shown in Section II-A, the current is determined by measuring the secondary current i_s at time instants t_2 and t_6, when the magnetic field strength in the

core equals $\pm H_c$. The increase in secondary current around H_c is small because the core is not saturated, hence its inductance value

$$L = \mu_r \mu_0 N_s^2 \cdot \frac{A_m}{l_m} \qquad (5)$$

where μ_0 is the magnetic constant and A_m is the cross section of the core, is proportional to the relative permeability μ_r. Hence, the slope of the secondary current

$$\frac{di_s}{dt} = \frac{v_L}{L} \qquad (6)$$

can be reduced by increasing the relative permeability μ_r. This helps to decrease the measurement error, which is introduced if i_s is measured slightly too early or late.

2) Coercive Magnetic Field Strength H_c: In many other current measurement concepts utilizing two-winding inductors, the coercive magnetic field strength H_c causes a measurement error [22]. As pointed out in Section II-B, this error is compensated in the presented concept by measuring i_{s1} and i_{s2}. Still, $|H_c|$ should be chosen as small as possible in order to reduce the losses and thus the self-heating of the core when traversing the hysteresis loop.

3) Saturation Magnetic Field Strength H_{sat}: As explained in Section II-A, the core needs to be saturated for a precise measurement of the primary current. Hence, H_{sat} should be as small as possible as can be shown by

$$i_p > i_{p,min} = \frac{l_m}{N_p} \cdot H_{sat}. \qquad (7)$$

4) Saturation Flux Density B_{sat}: B_{sat} influences the time needed to traverse the full hysteresis loop and thus the measurement frequency f according to

$$f = \frac{1}{\Delta t} = \frac{v_L}{\Delta B A_m N_s}. \qquad (8)$$

Assuming that it is not desired to provide a separate dc–dc converter for the current measurement system, v_L is given by V_{cc}, i.e., by the available voltage levels of the signal electronics. (Here, a value of $V_{cc} = 12$ V, as typical for the automotive industry, is chosen.) Hence, for a fast current measurement, a small B_{sat} is desirable. The measurement frequency can also be adjusted using the product $A_m N_s$.

5) Number of Primary Turns N_p: It is desirable to design the measurement system such that one primary turn $N_p = 1$ is sufficient as this allows to position the core easily on the pin of a power semiconductor package [cf., Fig. 1(a)].

6) Number of Secondary Turns N_s: For one primary turn, the number of secondary turns

$$N_s = \frac{i_p}{i_s} \qquad (9)$$

determines the level of the secondary current that is measured using the shunt R_s and needs to be switched by the H-bridge.

7) Core Cross Section A_m: A_m is inversely proportional to the measurement frequency as can be seen from (8) and hence should be chosen as small as manufacturing issues and the minimum required mechanical strength allow.

8) Length of the Magnetic Path l_m: According to (7), the length of the magnetic path l_m is directly proportional to the minimum current that can be measured and hence should be chosen as small as possible. Lower limits are introduced by the space consumed by the primary current carrying conductor and the secondary winding and by the required mechanical strength of the core.

III. REALIZATION OF MEASUREMENT SYSTEM

Having presented the working principle and important design parameters of the current measurement, in the following section the realized measurement system is described. The specifications of the realized systems include in addition to the temperature levels already mentioned in the introduction a current measurement range from -50 to 50 A and a measurement frequency of at least 50 kHz. The number of secondary turns is chosen to $N_s = 50$ to limit the current in the H-bridge to 1 A. This allows a reasonable silicon chip size of the switches even at an ambient temperature of $120\,°C$ (here, the two half-bridges are packaged each in an SO-8 package with an upper junction temperature limit of $175\,°C$). Furthermore, it reduces the wire diameter needed for the secondary winding and thus helps to achieve a low l_m.

A. Choice of Core Material

The nanocrystalline material Vacuumschmelze "Vitroperm 500F" is chosen for this example design as it features a high relative permeability up to $\mu_r = 150\,000$, a low coercive and saturation magnetic field strength as well as a comparably high temperature invariance of these magnetic parameters which is of great importance when designing a measurement system with a temperature difference during operation of more than 300 K (-40 to $250\,°C$ ambient temperature plus self-heating due to losses). These characteristic values can be derived from Fig. 7 showing the hysteresis loop measured at 25 kHz (which matches the excitation frequency of the hysteresis loop for a measurement frequency of 50 kHz) and 25 and $250\,°C$ using a "T60006-L2009-W914" core [23].

Even though the Curie temperature T_C of this material is higher than $600\,°C$, the manufacturer specifies an upper operating temperature limit of $155\,°C$ for the "Vitroperm" cores. This is primarily due to the epoxy coating or plastic casing of the cores. At temperatures above $300\,°C$, which are still significantly below T_C, the material starts to loose its nanocrystalline structure resulting in derated performance especially with respect to eddy current losses and hence, it has to be made sure that the material temperature does not rise significantly above $300\,°C$ for a longer period of time.

B. Choice of Core Dimensions

The smallest commercially available "Vitroperm 500F" core ("T60006-L2009-W914," which has already been used for measuring the hysteresis loop in Fig. 7), shows a magnetic path length of $l_m = 26\,mm$ and a cross section of $A_m = 6\,mm^2$. This leads to an undesirably high minimum current that can be
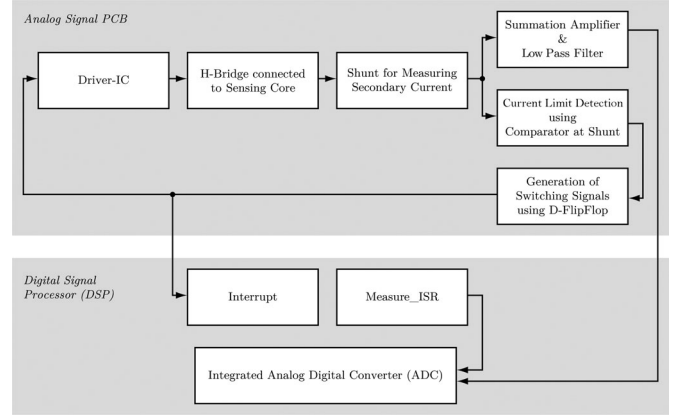
Fig. 8. Signal flow diagram for the analog control of the current measurement system and for the measurement routine within a DSP.
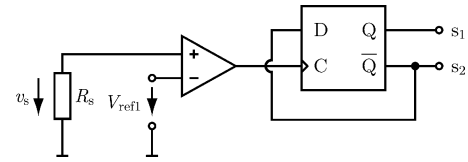
Fig. 9. Generation of switching signals for the H-bridge by comparing the shunt voltage v_s with a reference voltage V_{ref1}: output of the comparator (National Semiconductor "LM360") is fed to the clock input of a D flip-flop (Texas Instruments "CD74HCT74M"), the inverted output of which is connected to the D input of the flip-flop.

measured and a relatively long time needed for traversing the hysteresis loop, as can be seen in (7) and (8), respectively.

However, the cores in the plastic casing can be opened and the tape wound core can be unwound and then rewound with a smaller radius and less turns (leading to a lower l_m and A_m). For rewinding, the number N_t of tape turns "Vitroperm 500F" tape turns can be calculated using (8) to

$$N_t = \frac{A_m}{h_t d_t} = \frac{\Delta t v_L}{h_t d_t \Delta B N_s} = 21 \qquad (10)$$

for $v_L \approx 11$ V (V_{cc} is reduced by ohmic voltage drops), $\Delta B = 2.3$ T (cf. Fig. 7), and $\Delta t = 20\mu s$ (leading to a measurement frequency of 50 kHz due to the sampling scheme described in Section III-D), a height of the tape of $h_t = 4.4mm$ and a thickness of $d_t = 20\mu m$. This results in $A_m = 1.9\,mm^2$ and $l_m = 13.8mm$ and leads with (7) to a minimum measurable current of $i_{p,min} = 0.28A$ for $H_{sat} \approx 20$ A/m as a worst-case scenario at $250\,°C$ according to Fig. 7.

C. Signal Electronics

The structure of the signal electronics of the realized current measurement system is shown in Fig. 8: A PCB for the analog part containing the H-bridge (two Vishay Intertechnology "Si4946BEY" bridge legs [24]) and its gate drivers (Allegro Microsystems "A4940" [25]) is used to excite the core from the secondary side and a digital signal processor (DSP) mounted on a
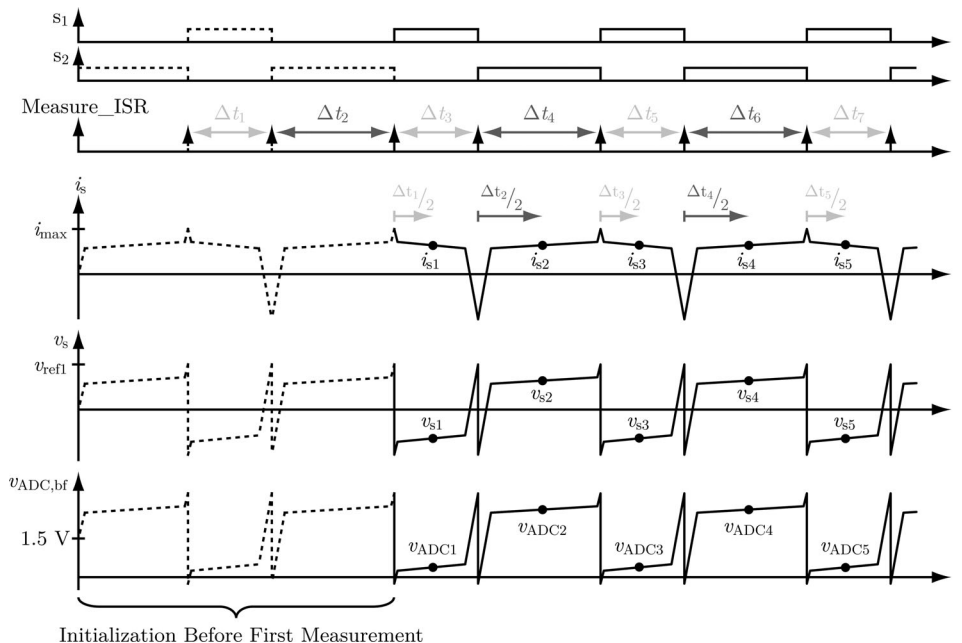
Fig. 10. Switching signals s_1 and s_2 generated by the circuit shown in Fig. 9 and the interrupts triggering the DSP routine "Measure_ISR" to start the counters needed to determine the correct point in time when to sample the adjusted shunt voltage applied to the ADC of the DSP are shown. Furthermore, the secondary current i_s of the bidirectionally saturated current transformer, the shunt voltage v_s, and the voltage $v_{\mathrm{ADC,bf}}$ applied to a low-pass filter and then to the ADC, are depicted.

separate PCB samples at certain points in time (cf. Section III-D) the scaled (to fit the input voltage range of the ADC of the DSP) and filtered shunt voltage v_s. The filtering of v_s is performed by an active second-order low-pass filter and is essential as measurement noise will otherwise cause false switching signals to be generated by the comparator (cf. the next paragraph). The voltage v_s itself and its scaled values (which correspond to the voltage v_{ADC} that is later filtered and applied to the ADC) are shown at the bottom of Fig. 10.

The switching signals (input signals of the gate driver) need to be generated very quickly after the core reaches saturation as the current rises very fast once it is saturated. Hence, they are not produced by the DSP but are generated by measuring the shunt voltage v_s and evaluating this voltage using a current limit detection circuit depicted in Fig. 9. The shunt voltage is compared to a reference voltage at a comparator. ($V_{\mathrm{ref1}} = 0.64$ V is chosen for this design, corresponding to a current through the 0.5 Ω shunt of 1.28 A making sure even with a maximum primary current of 50 A the secondary current can saturate the core in the direction opposing the primary current with $N_s = 50$ turns.) The output of the comparator is fed to the clock input of a D flip-flop, the inverted output of which is connected to the D input of the flip-flop. Hence, every time the shunt voltage increases above V_{ref1}, the rising clock edge makes the flip-flop toggle the output which is used as the switching signals for the n-MOSFET pairs T_1 and T_4 as well as T_2 and T_3.

D. Measurement Algorithm

The correct time instants t_2 and t_6 to measure the secondary currents i_{s1} and i_{s2} [cf. Fig. 5(b)], i.e., to sample the shunt voltage v_s, are determined by the interrupt service rou-

tine "Measure_ISR," which is started by an interrupt generated by the output toggling of the flip-flop. Right at the start of the routine, a timer is restarted to measure the time interval $\Delta t_i, 1 \leq i \leq 6, i \in \mathbf{N}$, between two consecutive interrupts (cf. Fig. 10). The interval that has been measured two interrupts before is cut in half to determine when to sample v_s. For example, in the interval Δt_3 in Fig. 10, the secondary current is measured when $\Delta t_1/2$ has elapsed. Hence, a measured current value can be provided twice per switching cycle of the H-bridge, e.g., twice per bidirectional traversing of the hysteresis loop. Furthermore, at the beginning of the current measurement (e.g., during start-up of the power electronic converter), the routine needs 1.5 pulse periods of the H-bridge ($\approx$50 μs) to initialize the variables where the counter values are stored in.

This way of determining when to measure the secondary current relies on two assumptions, which are validated with experimental results showing the measurement error in Fig. 14 in Section IV.

First, it is assumed that the time intervals when the core is saturated, i.e., from t_0 to t_1, from t_3 to t_5 and from t_7 to t_9 in Fig. 5(b) are small compared to the intervals t_1 to t_3 and t_5 to t_7 when the core is not saturated. This is fulfilled if the employed core shows a high relative permeability (cf. Section II-C). This allows also to use standard clocks and timers in the DSP as small inaccuracies in the timing will not introduce large errors. This is the main reason, why the switching signals are generated directly by the signal electronics (cf. Section III-C) and not by the DSP.

Second, this way of determining the point ($\pm H_c, 0$) in the H–B plane works precisely only if the current does not change significantly within the interval between three interrupts. As an interrupt occurs in the current design every 7 to 14 μs and the
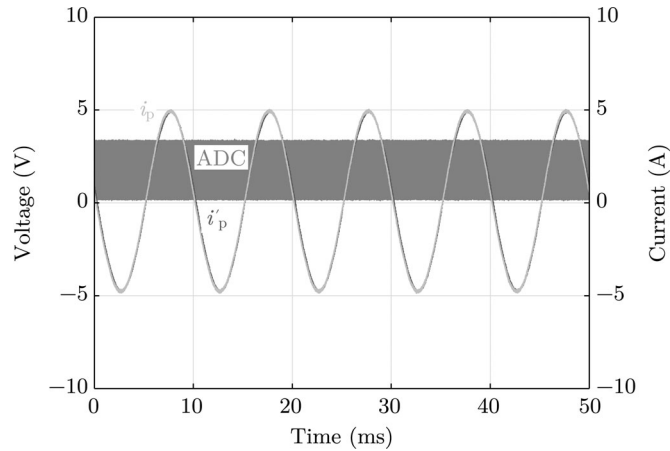
Fig. 11. Primary current measured with a wide band power analyzer (waveform denoted with i_p) and with the presented bidirectionally saturated current transformer (waveform denoted with i'_p). Also shown is the signal triggering the ADC.
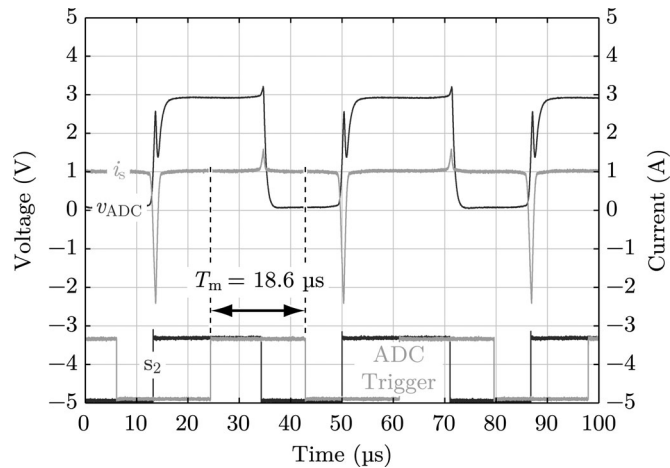

Fig. 13. Measured waveforms at 250 °C ambient temperature of the core: voltage v_{ADC} at the ADC of the DSP, shunt current i_s, switching signal s_2, and the software trigger starting the ADC conversion, with the latter two, s_2 and the ADC trigger, plotted with a negative offset of 5 V and scaled by a factor of 0.5 for the sake of clarity. The signals look as expected from the theoretical considerations in Fig. 10. Every 15.5 μs, corresponding to a measurement frequency of 67 kHz, a new current value is calculated.

Fig. 12. Measured waveforms at 25 °C ambient temperature of the core: voltage v_{ADC} at the ADC of the DSP, shunt current i_s, switching signal s_2, and the software trigger starting the ADC conversion, with the latter two, s_2 and the ADC trigger, plotted with a negative offset of 5 V and scaled by a factor of 0.5 for the sake of clarity. The signals look as expected from the theoretical considerations in Fig. 10. Every 18.6μs, corresponding to a measurement frequency of 54 kHz, a new current value is calculated.

maximum frequency of the sinusoidal currents that are to be measured is 1 kHz, only very small errors are introduced (cf. Fig. 14 in Section IV).

IV. EXPERIMENTAL RESULTS

In this section, the design and the previous theoretical considerations are experimentally verified using the measurement setup described in Section III. Fig. 11 shows the measurement of a sinusoidal ac current. The theoretical waveforms shown in Fig. 10 can be directly compared with the experimental waveforms in Figs. 12 and 13, measured at room temperature
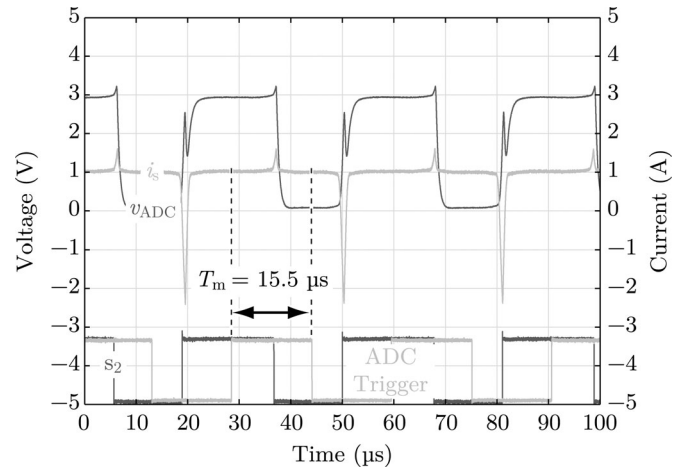
and at an ambient temperature around the core of 250 °C. The secondary current looks as expected, the ADC voltage is in the oscilloscope pictures in Figs. 12 and 13 directly measured at the ADC inputs (i.e., after the low-pass filter which is used to avoid large-voltage spikes on the signal) and the software trigger for starting the analog–digital conversion is shown in order to indicate the points in time when the shunt voltage is sampled. It can be seen that at room temperature the software outputs an updated value of the measured primary current every 18.6μs, corresponding to a measurement frequency of 54 kHz. At 250 °C, this values increases to 67 kHz due to the decreasing saturation flux density B_{sat} of the core [cf., (8) and Fig. 7].

The measurement error is determined by a reference measurement of the primary current using a wide band power analyzer ("D6100" by Norma) with a 0.03% precision shunt. The absolute error of the described system scales linearly with the measured current, starting from an absolute error of 0.065 A at a primary current of 2.5 A to an error of 1.2 A to 47.5 A. Hence, the relative error is constantly at around 2.5%. This error is mainly due to the use of resistors (for the shunt and voltage-level adjustment of the shunt voltage for the ADC, cf. Section III-C) that have a tolerance of their resistance around 1% and parasitic resistances of PCB tracks: a 10-mm-long and 1-mm-wide track shows a resistance of 4.8 mΩ, corresponding to 1% of the shunt resistor value.

As the primary current is calculated using the difference of two shunt voltages, errors due to offsets of, e.g., the operational amplifiers used cancel out to a large extent. Hence, the linear error can be compensated in the software. The resulting absolute and relative measurement errors are shown in Fig. 14. The remaining error of less than 0.5% is due to the slight inaccuracies introduced by the measurement algorithm as expected in Section III-D.
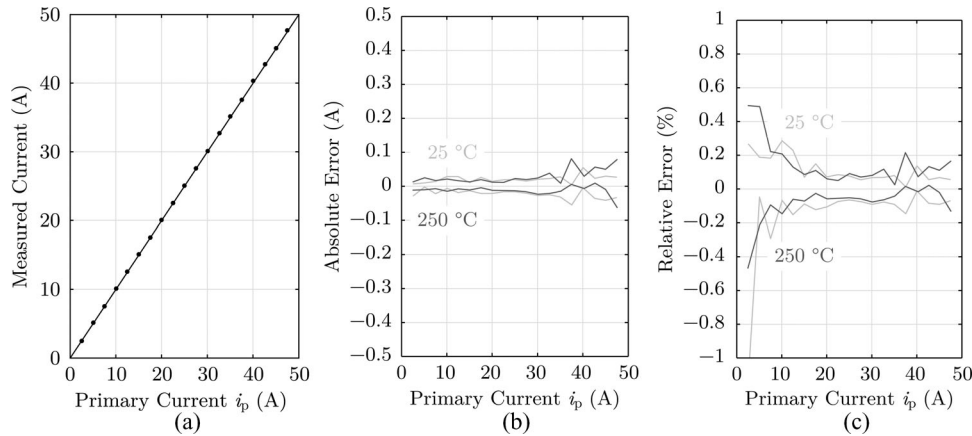
Fig. 14. Minimum and maximum absolute (cf. (a)) and relative (cf. (b)) measurement error of the proposed current measurement system over the full measurement range after this setup has been initially calibrated to compensate for the linearity error introduced by tolerances of resistance values.

V. CONCLUSION

In this paper, first the upcoming demand for high temperature power electronic converters and particularly for fast measurement of dc and sinusoidal ac currents is described. Subsequently, the measurement principle of a novel concept called "bidirectionally saturated current transformer," that is able to measure dc and sinusoidal ac up to 1 kHz and 50 A at an ambient temperature of up to 250 °C, is explained in detail.

The important design guidelines for choosing a core material (high μ_r, low H_c, H_{sat}, B_{sat}) and the magnetic design (high N_s, low N_p, A_m, l_m) are derived and an experimental prototype is practically realized accordingly. The required signal electronics consisting of a current limit detection that controls the H-bridge, which the secondary winding is connected to, and a circuit with a low-pass filter that also adjusts the voltage level of the shunt voltage which is sampled by the ADC of a DSP. Finally, measurements verifying the proposed concepts are provided and show a relative error of 2.6% and less than 0.5% after calibration even at 250 °C.

REFERENCES

[1] B. Wrzecionko, L. Steinmann, and J. W. Kolar, "Fast high-temperature (250° C/500° F) isolated dc and ac current measurement: Bidirectionally saturated current transformer," in *Proc. 7th Int. Power Electron. Motion Control Conf. (IPEMC 2012)*, vol. 1, Harbin, China, Jun. 2–5, 2012, pp. 480–487.

[2] R. Wang, D. Boroyevich, P. Ning, Z. Wang, F. Wang, P. Mattavelli, K. Ngo, and K. Rajashekara, "A high-temperature SiC three-phase ac-dc converter design for > 100 ° C ambient temperature," *IEEE Trans. Power Electron.*, vol. 28, no. 1, pp. 555–572, Jan. 2013.

[3] M. Huque, S. Islam, L. Tolbert, and B. Blalock, "A 200 ° C universal gate driver integrated circuit for extreme environment applications," *IEEE Trans. Power Electron.*, vol. 27, no. 9, pp. 4153–4162, Sep. 2012.

[4] J. Valle-Mayorga, C. Gutshall, K. Phan, I. Escorcia-Carranza, H. Mantooth, B. Reese, M. Schupbach, and A. Lostetter, "High-temperature silicon-on-insulator gate driver for SiC-FET power modules," *IEEE Trans. Power Electron.*, vol. 27, no. 11, pp. 4417–4424, Nov. 2012.

[5] F. Renken and R. Knorr, "High temperature electronic for future hybrid powertrain application," in *Proc. Eur. Conf. Power Electron. Appl.*, Dresden, Germany, Sep. 11–14, 2005.

[6] S. Pischinger, M. Pischinger, H. Kemper, and S. Christiaens, "The challenges of system integration of the hybrid electric powertrain," in *Fachtagungsberichte VDE Kongress*, Aachen, Germany, Oct. 23–25, 2006.

[7] G. A. Landis, "Robotic exploration of the surface and atmosphere of Venus," *Acta Astronautica*, vol. 59, no. 7, pp. 570–579, 2006.

[8] A. König, "High temperature dc-to-dc converters for downhole applications," Ph.D. dissertation, Inst. Power Electron. and Electrical Drives, RWTH Aachen University, Aachen, Germany, Jun. 2009.

[9] S. Matsumoto, "Advancement of hybrid vehicle technology," in *Proc. Eur. Conf. Power Electron. Appl.*, Dresden, Germany, Sep. 11–14, 2005.

[10] B. J. Baliga, *Fundamentals of Power Semiconductor Devices*. New York, NY, USA: Springer Science + Business Media, 2008.

[11] T. Funaki, J. C. Balda, J. Junghans, A. S. Kashyap, H. A. Mantooth, F. Barlow, T. Kimoto, and T. Hikihara, "Power conversion with SiC devices at extremely high ambient temperatures," *IEEE Trans. Power Electron.*, vol. 22, no. 4, pp. 1321–1329, Jul. 2007.

[12] J. G. Bai, J. Yin, Z. Zhang, G.-Q. Lu, and J. D. van Wyk, "High-temperature operation of SiC power devices by low-temperature sintered silver die-attachment," *IEEE Trans. Adv. Packag.*, vol. 30, no. 3, pp. 506–510, Aug. 2007.

[13] E. Schulze, C. Mertens, and A. Lindemann, "Pure low temperature joining technique power module for automotive production needs," in *Proc. 6th Int. Conf. Integr. Power Electron. Syst.*, Nuremberg, Germany, Mar. 16–18, 2010, pp. 333–338.

[14] P. Ning, F. Wang, and K. Ngo, "High-temperature SiC power module electrical evaluation procedure," *IEEE Trans. Power Electron.*, vol. 26, no. 11, pp. 3079–3083, Nov. 2011.

[15] D. Bortis, B. Wrzecionko, and J. W. Kolar, "A 120 ° C ambient temperature forced air-cooled normally-off SiC JFET automotive inverter system," in *Proc. 26th Annu. IEEE Appl. Power Electron. Conf. Expo.*, Fort Worth, TX, USA, Mar. 6–10, 2011, pp. 1282–1289.

[16] B. Wrzecionko, J. Biela, and J. W. Kolar, "SiC power semiconductors in HEVs: Influence of junction temperature on power density, chip utilization and efficiency," in *Proc. 35th Annu. Conf. IEEE Ind. Electron. Soc.*, Porto, Portugal, Nov. 3–5, 2009, pp. 3834–3841.

[17] HALA Contec GmbH & Co. KG, Ottobrunn, Germany. (2010, Oct.). *Thermal Navigator*. [Online]. Available: http://www.hala-tec.com/mod_use/dokumente/Thermal-Navigator_en.pdf

[18] B. Wrzecionko, A. Looser, J. W. Kolar, and M. Casey, "High-temperature (250 ° C/500 ° F) 19 000 r/min BLDC fan for forced air-cooling of advanced automotive power electronics," in *Proc. 37th Annu. Conf. IEEE Ind. Electron. Soc.*, Melbourne, Australia, Nov. 7–10, 2011, pp. 4162–4169.

[19] P. Ning, F. Wang, and K. D. T. Ngo, "250 °C SiC high density power module development," in *Proc. 26th Annu. IEEE Appl. Power Electron. Conf. Expo.*, Fort Worth, TX, USA, Mar. 6–10, 2011, pp. 1275–1281.

[20] J. R. Leehey, L. Kushner, and W. S. Brown, "DC current transformer," in *Proc. 13th Annu. Power Electron. Spec. Conf.*, Cambridge, MA, USA, Jun. 14–17, 1982, pp. 438–444.

[21] D. Azzoni, W. Teppan, and M. Carpita, "An innovative low-cost, high performance current transducer for battery monitoring applications: Prototype preliminary results," in *Proc. Int. Power Convers. Intell. Motion Conf.*, Nuremberg, Germany, May 12–14, 2009, pp. 443–449.

[22] J. A. Houldsworth, "Purpose-designed ferrite toroids for isolated current measurement in power electronic equipment," in *Proc. 4th Annu. Power Convers. Int. Conf.*, San Francisco, CA, USA, Mar. 29–31, 1982, pp. 101–109.

[23] (2010). *Nanocrystalline Vitroperm EMC Products*, Vacuumschmelze GmbH & Co. KG, Grüner Weg 37, 63450 Hanau, Germany. [Online]. Available: http://www.vacuumschmelze.com/fileadmin/Medienbiliothek _2010/Downloads/KB/Vitroperm_EMV_EN_full.pdf

[24] Vishay Intertechnology, Inc. (2009, Nov. 16). *Dual N-Channel 60 V (D-S) 175 °C MOSFET*. [Online]. Available: http://www.vishay.com/docs/ 73411/si4946be.pdf

[25] Allegro MicroSystems, Inc., *Automotive Full Bridge MOSFET Driver*, Rev. 1 ed., Allegro MicroSystems, Inc., (2009). [Online]. Available: http:// www.allegromicro.com/Products/Motor-Driver-And-Interface-ICs/ Brush-DC-Motor-Drivers//media/Files/Datasheets/A4940- Datasheet.ashx

Benjamin Wrzecionko (S'08) received the Dipl.-Ing. degree from RWTH Aachen University, Aachen, Germany, in 2008 after his studies in electrical engineering at RWTH Aachen University and at the University of Bath, Bath, U.K. He is currently working toward the Ph.D. degree at the Power Electronic Systems Laboratory, ETH Zurich, Zurich, Switzerland.

He worked in the serial development of Hybrid Electric Vehicles at a large German car manufacturer and developed a galvanically isolated dc–dc converter for hybrid electric and fuel cell vehicles at the power electronic systems laboratory of Swiss Federal Institute of Technology (ETH) Zurich, Zurich, Switzerland. His research interests for the Ph.D. dissertation include ultracompact, high temperature traction drive converter systems for HEVs using novel SiC power semiconductors.

Lukas Steinmann was born in Grabs, Switzerland, on December 25, 1984. He received the M.Sc. degree in electrical engineering from the Swiss Federal Institute of Technology (ETH Zurich), Zurich, Switzerland in 2011. In his diploma thesis, he dealt with high-temperature current measurement at the Power Electronic Systems Laboratory, ETH Zurich. During the Master Program at ETH Zurich, he focused on micro- and optoelectronics.

He worked in the field of analog electronics for an independent supplier of space technology as a four-month internship in 2009. Since 2012, he is working as a Process Engineer for humidity and temperature sensors at a company in Stäfa, Switzerland.

Johann W. Kolar (F'10) received the M.Sc. and Ph.D. degrees (*summa cum laude/promotio sub auspiciis praesidentis rei publicae*) from the Vienna University of Technology, Vienna, Austria.

Since 1982, he has been an independent international consultant in close collaboration with the Vienna University of Technology, Vienna, in the fields of power electronics, industrial electronics, and high-performance drives. He has proposed numerous novel converter topologies and modulation/control concepts, e.g., the VIENNA rectifier, the SWISS rectifier, and the three-phase ac–ac sparse matrix converter. He has published more than 400 scientific papers at main international conferences, more than 150 papers in international journals, and 2 book chapters. Furthermore, he has filed more than 110 patents. He joined as an Associate Professor and Head of the Power Electronic Systems Laboratory at the Swiss Federal Institute of Technology (ETH) Zurich on February 1, 2001, and was promoted to the rank of Full Professor in 2004. Since 2001, he has supervised more than 60 Ph.D. students and Postdoctoral Fellows. His current research interests include ac–ac and ac–dc converter topologies with low effects on the mains, e.g., for data centers, more-electric-aircraft and distributed renewable energy systems, and on solid-state transformers for smart microgrid systems. Further main research areas are the realization of ultracompact and ultraefficient converter modules employing latest power semiconductor technology (SiC and GaN), micropower electronics and/or power supplies on chip, multidomain/scale modeling/simulation and multiobjective optimization, physical model-based lifetime prediction, pulsed power, and ultrahigh speed and bearingless motors. He joined as an IEEE Distinguished Lecturer at the IEEE Power Electronics Society in 2011. He initiated and/or is the founder/cofounder of four spin-off companies targeting ultrahigh speed drives, multidomain/level simulation, ultracompact/efficient converter systems, and pulsed power/electronic energy processing. In 2006, the European Power Supplies Manufacturers Association (EPSMA) awarded the Power Electronics Systems Laboratory of ETH Zurich as the leading academic research institution in Power Electronics in Europe.

Dr. Kolar is a Member of the IEEJ and of International Steering Committees and Technical Program Committees of numerous international conferences in the field (e.g., the Director of the Power Quality Branch of the International Conference on Power Conversion and Intelligent Motion). He is the Founding Chairman of the IEEE PELS Austria and Switzerland Chapter and Chairman of the Education Chapter of the EPE Association. From 1997 to 2000, he served as an Associate Editor of the IEEE TRANSACTIONS ON INDUSTRIAL ELECTRONICS and since 2001 he has been serving as an Associate Editor of the IEEE TRANSACTIONS ON POWER ELECTRONICS. Since 2002, he has been an Associate Editor of the *Journal of Power Electronics of the Korean Institute of Power Electronics* and a Member of the Editorial Advisory Board of the *IEEJ Transactions on Electrical and Electronic Engineering*. He received seven IEEE Transactions Prize Paper Awards and seven IEEE Conference Prize Paper Awards. Furthermore, he received the ETH Zurich Golden Owl Award 2011 for Excellence in Teaching and an Erskine Fellowship from the University of Canterbury, New Zealand, in 2003.